ETH
Eidgenössische Technische Hochschule Zürich
Swiss Federal Institute of Technology Zurich

Design of a compact 2D magneto-optical trap for loading ion traps

Master thesis

ETH Zurich

MARTIN NORBERT WOSCHANK

DEPARTMENT OF PHYSICS

INSTITUTE FOR QUANTUM ELECTRONICS

TRAPPED ION QUANTUM INFORMATION GROUP

SUPERVISORS:

MSc. ROLAND MATT

DR. MATTHEW GRAU

PROF. JONATHAN HOME

Contents

Abstract

In this thesis, I present a design for a simple and compact two-dimensional magneto-optical trap (2D-MOT). This serves as a source of slow atoms to load ion-traps. The high heat load by using conventional ovens has been discussed extensively [30]. An ablation oven relies on a high-power laser, which is expensive [6]. This can be avoided by introducing a 2D-MOT [11, 24]. The temperature of the atoms, coming out of the oven and the ones, being slowed down and confined within the magneto-optical field, have been determined via the Doppler broadened linewidth. Furthermore, a novel design of an oven is presented. A long operating time of approximately 10000 h has been calculated.

Introduction

Trapped ions are a promising candidate for quantum information processing. Various methods and trap designs based on the combination of static electric fields and oscillating electric and static magnetic fields have been demonstrated [12, 25, 27]. There are several options of loading ion traps like effusion ovens, ablation ovens, Zeeman slowers and MOTs [29, 30, 6, 10, 8, 7, 21]. An ideal solution for loading ion traps would be non-intrusive, like no heat load and trap contamination. The broad velocity distribution in effusion ovens give heat loads and while ablation ovens and Zeeman slowers have lower heat loads, they are more complex [6, 14, 22]. Therefore, a simple and robust setup is desired. The 2D-MOT, used in this work, is such a system [28, 11].

After a short introduction into the field of laser cooling, I will describe Doppler cooling on the example of an optical molasses system [16, 20]. Section 1.3 introduces a magnetic quadrupole field and circularly polarized light to explain a MOT system with focus on a 2D-MOT. This is followed by the introduction of Calcium (Ca) as suitable candidate for quantum operations. Chapter 2 shows the apparatus, including the oven, vacuum system and optics. This is followed by a quantitative Monte-Carlo simulation of the 2D-MOT system in Chapter 3. Chapter 4 discusses the measurement results. Finally, a summary and further outlook are given.

Chapter 1

Theoretical description of a magneto-optical trap

In this chapter, I give a theoretical description of the physics within a MOT, with a focus on atomic neutral Ca. Section 1.1 describes the mathematical principles behind laser cooling. Section 1.2 introduces an optical molasses system. This gives the framework for a MOT in Section 1.3. Finally, I introduce some properties of Ca and explain why it is used in this setup.

1.1 Mathematical description of laser cooling

Laser cooling is a way of reducing the motional energy of atoms due to momentum transfer from atoms to light during off-resonant scattering, as described in Ref. [17, 26, 5]. For simplicity, only a photon-atom interaction is considered, with the photon described by a single-frequency light field and the atom by a two-level system. I will focus on an atom at rest, interacting with either a standing, or a traveling wave. The force on an atom interacting with light has been derived in Ref. [17, P. 30].

~~The force on an atom can be expressed by~~

$$\mathrm{F} = \left\langle \frac{\partial \hat{\mathcal{H}}}{\partial \mathrm{z}} \right\rangle . \tag{1.1}$$

For a light field, the interaction Hamiltonian is

$$\hat{\mathcal{H}}\prime = -\mathrm{e}\tilde{\mathrm{E}}(\tilde{\mathrm{r}}, \mathrm{t})\tilde{\mathrm{r}} \, , \tag{1.2}$$

where $\vec{E}(\vec{r}, t)$ is the electrical field of the light and $\vec{r}$ the distance of that dipole.

The Rabi frequency Ω and its derivative $\frac{\partial \Omega}{\partial z}$ are

$$\Omega = \frac{-\mathrm{eE(z)}}{\hbar} \langle \mathrm{e}|\mathrm{r}|\mathrm{g} \rangle \tag{1.3}$$

and

$$\frac{\partial \Omega}{\partial \mathrm{z}} = (\mathrm{q_r} + \mathrm{i}\mathrm{q_i})\Omega \, . \tag{1.4}$$

The logarithmic derivative of Ω are split up into a real and imaginary part, because the Rabi frequency can be complex, too.

q_r (q_i) is the real (imaginary) part of the derivative of Ω with respect to z.

$$\mathrm{q_r} = \mathrm{Re} \left(\frac{1}{\Omega} \frac{\partial \Omega}{\partial \mathrm{z}} \right) \tag{1.5}$$

$$\mathrm{q_i} = \mathrm{Im} \left(\frac{1}{\Omega} \frac{\partial \Omega}{\partial \mathrm{z}} \right) \tag{1.6}$$

The force on an atom, in z-direction, interacting with a light field is

$$\mathrm{F} = \hbar \mathrm{q_r} \left(\Omega \rho^*_{\mathrm{eg}} + \Omega^* \rho_{\mathrm{eg}} \right) + \mathrm{i}\hbar \mathrm{q_i} \left(\Omega \rho^*_{\mathrm{eg}} - \Omega^* \rho_{\mathrm{eg}} \right) , \tag{1.7}$$

~~ρ_{eg} describes the optical coherence between the ground and excited states,~~ whose are the off-diagonal elements of the density matrix.

The traveling wave, after applying the rotating wave approximation, is

$$\mathrm{E(z)} = \frac{\mathrm{E_0}}{2}\left(\mathrm{e^{i(kz-\omega t)}} + \mathrm{c.c}\right) . \tag{1.8}$$

By calculation of Eq. (1.4) with the electric field in Eq. (1.8) and the Rabi frequency in Eq. (1.3), a constant amplitude (q_r=0) and phase gradient (q_i=k) can be found.

In the case of a standing wave, the electric field is

$$\mathrm{E(z)} = \mathrm{E_0}\left(\mathrm{e^{-i\omega t}} + \mathrm{c.c}\right) . \tag{1.9}$$

This results in q_i=0 and $q_r = -k\tan(kz)$.

Substituting the solution of the optical Bloch equations [17] in steady-state,

$$\rho_{\mathrm{eg}} = \frac{\mathrm{i}\Omega}{2(\gamma/2 - \mathrm{i}\delta)(1+\mathrm{s})} , \tag{1.10}$$

into Eq. (1.7) gives

$$\mathrm{F} = \frac{\hbar \mathrm{s}}{1+\mathrm{s}}\left(-\delta \mathrm{q_r} + 1/2\gamma \mathrm{q_i}\right) . \tag{1.11}$$

The detuning δ is

$$\delta = \omega_{\mathrm{L}} - \omega_{\mathrm{A}} , \tag{1.12}$$

with ω_A the atomic transition frequency and ω_L the laser frequency.

In Eq. (1.11) the decay rate γ is

$$\gamma = \frac{1}{\tau} , \tag{1.13}$$

where τ expresses the lifetime of the exited state.

From Eq. (1.11), two forces can be derived, namely the scattering force (imaginary part) and the dipole force (real part).

The scattering force of a photon-atom spontaneous emission cycle comes from the momentum absorbed and emitted by an atom. This gives

$$\mathrm{F_{sp}} = \hbar \mathrm{k} \gamma \rho_{\mathrm{ee}} \,, \tag{1.14}$$

where ρ_{ee} is the excited state population defined by the optical Bloch equations. Therefore, by calculating Eq. (1.14), the scattering force is

$$\mathrm{F_{sp}} = \frac{\hbar \mathrm{k} \gamma}{2} \frac{\mathrm{s_0}}{1 + \mathrm{s_0} + (2\delta/\gamma)^2} \,. \tag{1.15}$$

The saturation parameter $\mathrm{s_0}$ is

$$\mathrm{s_0} = \frac{\mathrm{I}}{\mathrm{I_0}} \,, \tag{1.16}$$

where $\mathrm{I_0}=\frac{2\pi^2 hc\Gamma}{3\lambda^3}$ is the saturation intensity and I is the intensity of the laser [18].

The polarization of the light changes within a standing wave, composed of two counter-propagating beams, resulting in a spatially modulated light shift. This produces a dipole force, which has been derived in [17, P. 33] and is

$$\mathrm{F_{dip}} = \frac{2\hbar k \delta s_0 sin(2kz)}{1 + 4 s_0 cos^2(kz) + (2\delta/\gamma)^2} \,. \tag{1.17}$$

Eq. (1.15) can be related to the second term of Eq. (1.11) and Eq. (1.17) to the first term. Eq. (1.11) saturates at high intensities, because $\mathrm{s_0}$ becomes large. For high saturation $\mathrm{s_0}$»1, F_{sp} is

$$F_{sp} = \frac{\hbar k \gamma}{2} \,. \tag{1.18}$$

If the intensity gets higher, the ratio of stimulated emission to spontaneous emission gets higher. Stimulated emission does not cause cooling as it is directed along the absorbed photon direction.

1.2 Optical molasses

In this section, I will go through an optical molasses system and explain Doppler cooling, based on Ref. [16, 20].
An optical molasses system uses three perpendicular laser beam pairs to slow down particles. The main cooling mechanism is Doppler cooling. It describes cooling of a moving atom within a laser field, where its frequency is tuned below resonance ("red-detuned"), with respect to a desired transition, due to the Doppler shift. If an atom moves towards a resonant photon, the photons frequency is tuned above the resonant transition of the atom ("blue-detuned") in the reference frame of the atom. For a red-detuned laser beam, the absorption probability increases (see section 3). This results in the atom aquiring the photon's momentum. When the atom spontaneously emits a photon, the direction of the emitted photon is random. This results in a net increase of the atom's momentum in the laser beam direction, but no net increase in spontaneous emission. The increase of net momentum diminishes at higher intensities, because the ratio of stimulated emission events, where the emitted photon has the same momentum as the absorbed photon, to spontaneous emission increases. The force due to the laser beam photon traveling along the direction of the beam axis is

$$\tilde{\mathrm{F}}_{\pm} = \pm \frac{\hbar \tilde{\mathrm{k}} \gamma}{2} \frac{\mathrm{s}_0}{1 + \mathrm{s}_0 + (2(\delta \mp |\tilde{\mathrm{k}} * \tilde{\mathrm{v}}|)/\gamma)^2} \,. \tag{1.19}$$

The total scattering force $\vec{F}$ of the photon-atom interaction is

$$\tilde{\mathrm{F}} = \tilde{\mathrm{F}}_{+} + \tilde{\mathrm{F}}_{-} \,. \tag{1.20}$$

The amount of momentum that the atom absorbs from a photon determines the so-called Doppler limit, which is the minimum temperature $\mathrm{T}_{\mathrm{min}}$ achievable by Doppler cooling [20],

$$\mathrm{T}_{\mathrm{min}} = \frac{\hbar \Gamma}{2\mathrm{k}_{\mathrm{B}}} \,. \tag{1.21}$$

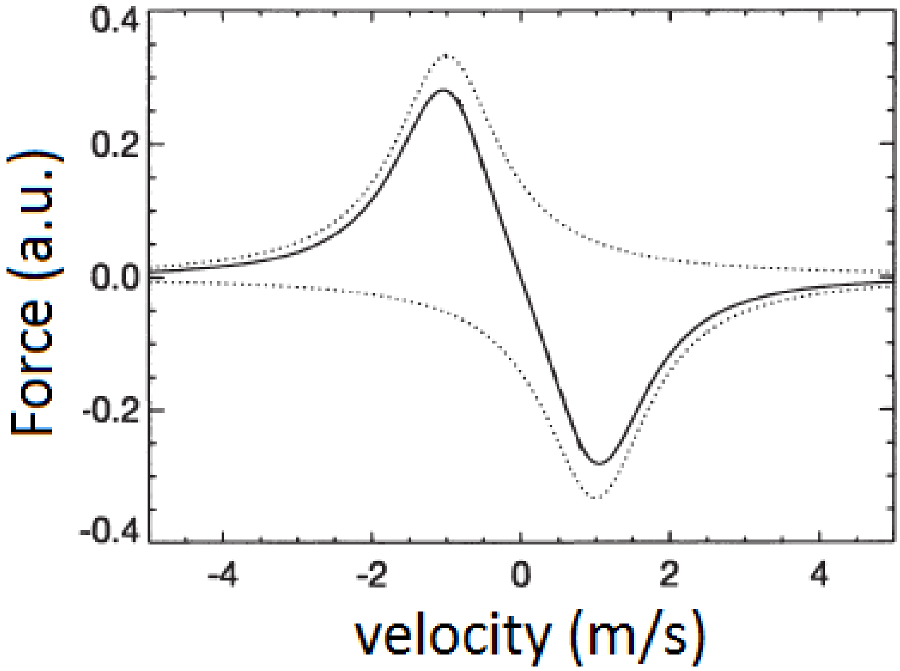

Figure 1.1: Plot of an atom traveling along the beam axis of an optical molasses taken from Ref. [16]. The net force (solid line) is the sum of the two counter-propagating laser beams (dotted lines). If the atom travels towards a photon, it experiences a repulsive force. As soon as the atom changes direction, the force also changes sign, always producing a force directed opposite to the velocity vector.

1.3 Magneto-optical trap

A MOT is a system, which uses a magnetic quadrupole-like field and counter-propagating laser beams to slow down or trap atoms. It is one of the most commonly used methods to trap neutral atoms. The system uses optical cycling, which describes the excitation from the ground state to an excited state and relaxation back onto this ground state.

The capture velocity v_c [2] is

$$\mathrm{v_c} = 1.43\sqrt{\frac{2\mathrm{U}}{\mathrm{m}}}\,. \tag{1.22}$$

The trap-depth is given by U and m is the mass of the atom.

Eq. (1.22) describes the upper velocity that atoms can have to be confined. Above this limit, the number of spontaneous emission cycles is too low and atoms escape. Optical cycling allows better control and loading of atoms, as long as the velocity of them is below the capture velocity of the MOT (see Ref. [17, 24]).

To be able to understand the scattering force of a MOT, we modify Eq. (1.19) by including a Zeeman shift,

$$\delta_{\mathrm{zeeman}} = \pm\mu'\mathrm{B}/\hbar\,. \tag{1.23}$$

Here, μ' is the effective magnetic moment.

$$\delta_{\pm} = \delta + \delta_{\mathrm{doppler}} + \delta_{\mathrm{zeeman}}\,. \tag{1.24}$$

where $\delta_{doppler}$=$\mp\vec{k}\vec{v}$ denotes the Doppler shift [17, P. 158].

Then, the scattering force gives

$$\tilde{F}_{\pm} = \pm \frac{\hbar \tilde{k} \gamma}{2} \frac{s_0}{1 + s_0 + (2\delta_{\pm}/\gamma)^2}\,, \tag{1.25}$$

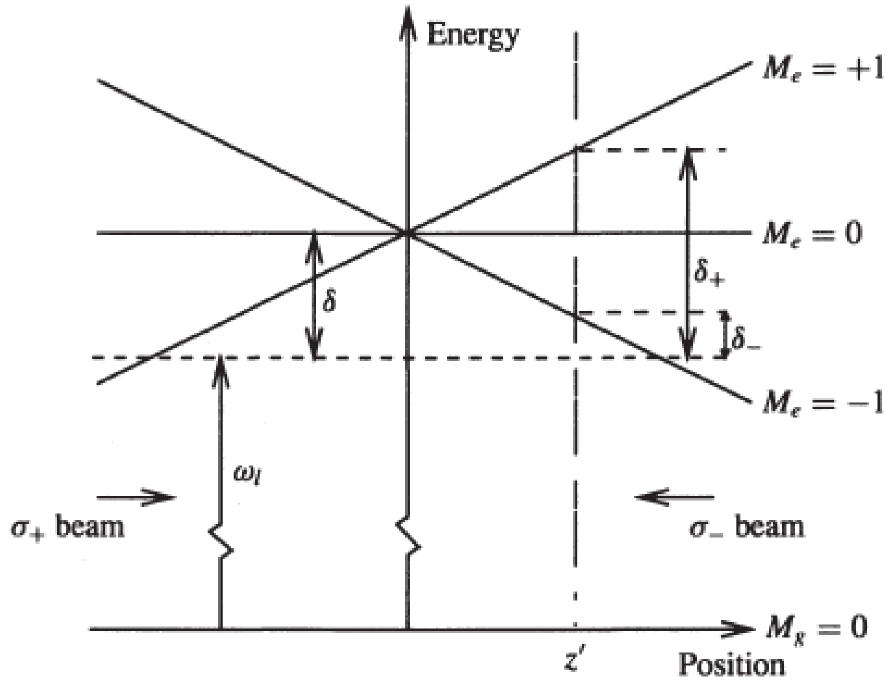

Figure 1.2: Magneto-optical trap in 1D taken from Ref. [17]. Energy of magnetic sub-levels ($M_g = 0, M_e = 0, \pm 1$) over position in a quadrupole magnetic field gradient with null at z=0. The black-dotted line shows the energy of the photon with frequency ω_l detuned by δ from M_l=0. σ^+ and σ^- denote the polarization of the incoming positively and negatively circular-polarized beams. δ_+ and δ_- describe the detuning from the frequency of the laser beams to the M_e=+1 and M_e=-1 magnetic sub-levels. The atoms further from the magnetic quadrupole null experience larger Zeeman shifts, resulting in a smaller effective laser detuning δ_- and an increased scattering rate. The laser propagation direction ensures that the scattering forces are always inward towards the quadrupole null.

The Zeeman shift term in equation (1.24) arises from sub-level splitting for M≠0 of an atom due to interaction with a magnetic field. If the magnetic field has a gradient, the splitting is position dependent.

The cooling process is implemented by two counter-propagating laser beams

~~of opposite circular polarization, σ^+ and σ^-. Both beams are detuned below~~ the M_g=0 M_e=±1 atomic transition for every position z', by δ.

In the case of 1 dimension, which can also be seen in Figure 1.2, for a magnetic field gradient ∇B>0, the state $M_e = +1(-1)$ will be shifted upwards (downwards). The magnetic field gradient shifts the ΔM=-1 transition closer to resonance. If, for any position z' (see Figure 1.2), the polarization of the right beam (see Figure 1.2) is chosen to be σ^- and σ^+ for the other one, the atoms are driven towards the center (B=0). Otherwise, they are moving away from the center. Therefore cooling and confinement of the atoms can be accomplished simultaneously. To put this into 2 dimensions, four instead of two laser beams are used.

1.3.1 Two dimensional magneto-optical trap

Within a 2D-MOT, the atoms are confined in the plane of the laser beams (x-y plane). There is no force, acting on the atom, in the direction of no laser beams through absorbing photons. The only contribution to the velocity on this axis comes from spontaneous emission.

Due to high pressures (p>10^{-6} mBar), the atom-atom interaction rate exceeds the photon-atom interaction rate and the MOT stops working.

1.4 Calcium atom

In the following, I will introduce neutral ^{40}Ca as promising candidate for laser cooling, based on Ref. [15, 9]. This Ca atoms will be ionized in order to do quantum information processing.
Ca belongs to the group of alkali-earth atoms. It has two valence electrons, and so it has a more complicated spectrum than Hydrogen-like atoms.

Table 1.1: Half life times, natural abundances and isotope shifts at cooling transition ($^1S_0$-$^1P_1$) relative to ^{40}Ca [20, P. 24]

Isotope	**Natural abundance (%)**	**Isotope shift (MHz)**	**Half life**
40	96.94	0	Stable
41	10^{-12}	166	10^5 Years
42	0.65	393	Stable
43	0.14	554	Stable
44	2.09	774	Stable
46	10^{-3}	1160	10^{15} Years
48	0.19	1513	$>10^{19}$ Years

^{40}Ca has an isotopic abundance of 97 percent (see Table 1.1).
The half life times in Table 1.1 can be considered to be stable. Calcium has transitions, which can be addressed with diode lasers and has no hyperfine splitting in the ground state of ^{40}Ca. In ^{41}Ca, the hyperfine splitting of the ground state give dark states in cooling. Like other alkali-earth atoms (Sr, Yb, Ba), Ca also has a ^{1}D meta-stable manifold (see Figure 1.3). This is not beneficial for laser cooling, because if an electron decays into this manifold of states (1 decay event in every 10^5), it will leave the cooling cycle and needs to be repumped by an additional laser at 671.9 nm. Due to the small branching ratio although, no repumping laser is needed.
The vapor pressure is

$$p = 5.006 + A + \frac{B}{T} + C \times \log(T) + \frac{D}{T^3} \text{Pascals}\,. \qquad (1.26)$$

A, B, C and D are the measured empirical values taken from Ref. [1].

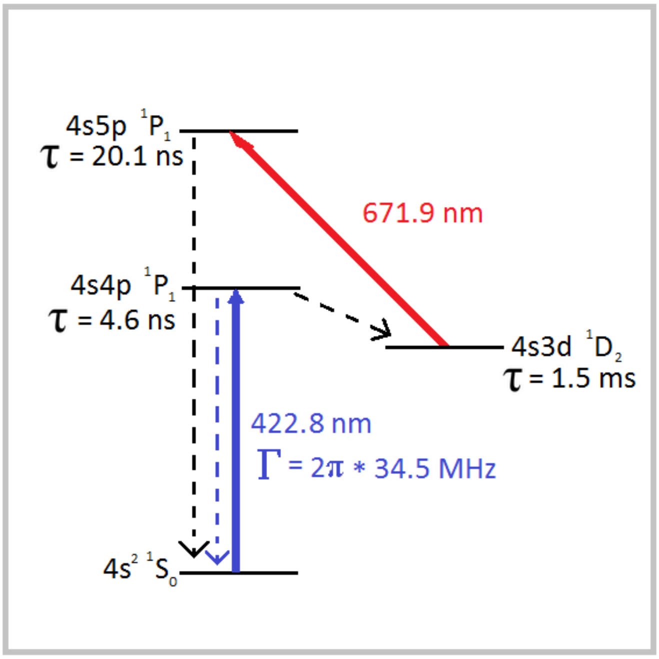

Figure 1.3: Simplified energy level diagram of ^{40}Ca. The radiative lifetime of the corresponding states τ is shown. The blue arrow shows the cyclic transition between the ground state $^1S_0$ and the excited state $^1P_1$. The red arrow shows the transition between the meta-stable state $^1D_2$ and the excited state 4s5p $^1P_1$, which can be used for repumping, if needed. The black dotted lines show the dipole allowed decays from the excited states to the lower states [20, 19]. The cycling transition at 422.8 nm with linewidth $\Gamma = 2\pi \times$ 34.5 MHz has a Doppler cooling limit of 3 mK [20]. The frequency of the cooling transition is given by 709.078373 THz [23].

For laser cooling Ca, the 4s^2 $^1S_0$ – 4s4p $^1P_1$ transition will be used, due to the short lifetime of the 4s4p $^1P_1$ level (see Figure 1.3). The small linewidth corresponds to a better isotope selectivity. After ionization, the Ca ion has only one valence electron, which yields to a simple energy level scheme and faster cooling. Furthermore, it still has a metastable state that can be used, e.g. for quantum state detection.

Chapter 2

Experimental setup

In this chapter, I will discuss the experimental apparatus, consisting of the oven, vacuum chamber and optics.

2.1 The oven

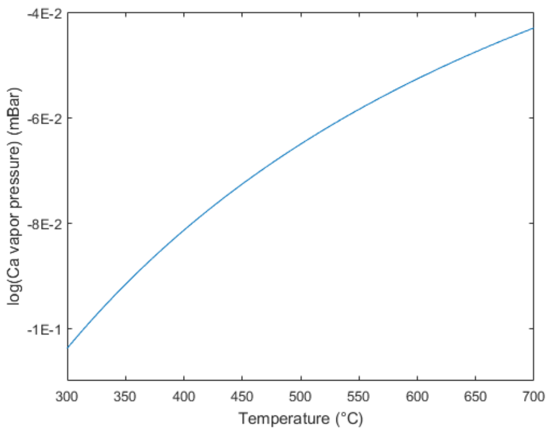

Figure 2.1: Vapor pressure of metallic Ca at a temperature between 300 °C and 700 °C by application of (1.4). The melting point of Ca is at 842 °C.

The oven needs to withstand temperatures around 500 °C, because at those temperatures, an appreciable vapor pressure for Ca is achieved (see Figure

2.1). Therefore, the oven used in this work is made out of a ceramic material, called Macor. This material can be used within UHV and at high temperatures, compared to other materials, like plastics. A vessel within the oven is filled by Ca granules and the Ca is directly heated up with a resistive wire made out of Constantan.

Figure 2.2: Explosion view of the oven parts. The upper most part is the solid angle of Ca coming out of the oven. The lid, shown next to the cone consists of four holes at the side. This serves the purpose of venting and being able to collimate the outcoming atomic beam. The next part is a block, which corresponds to Ca granules. The next part is the inner chamber. The holes lead the heating wire. Otherwise, the heating wire short circuits. The bottom part is the outer chamber. It has a slit for connecting the heating wire to the electrical feedthrough. On the inner wall of the outer chamber, four equally spaced edges hold the inner chamber in place.

2.1.1 Calculation of the oven output

To simulate the oven properly, the temperature of the output nozzle must be calculated. An assumption made is that the heating wire within the oven is a disk with a mean distance from the nozzle of half the oven height. The surface A_s of this disk is

$$A_s = 2r_s^2\pi + 2r_s\pi d_s, \tag{2.1}$$

with r_s as the radius of the disk and d_s the thickness.
The volume of the lid with nozzle is

$$V = r_m^2\pi d_m, \tag{2.2}$$

with r_m as the radius of the lid and d_m the thickness.
The dissipated radiation power from the disk follows from the Stefan-Boltzmann law,

$$P = A_s\sigma T_s^4, \tag{2.3}$$

with σ being the Boltzmann constant, A_s the surface of the source and T_s the temperature of the source. η includes the losses to get the absorbed power of the lid, given by

$$\eta = \alpha\frac{A_{mr}}{A_{sr}}. \tag{2.4}$$

α is the absorption coefficient, A_{mr} the surface that is hit by the radiation and A_{sr} the surface of our radiation source after a distance b.

$$\frac{\mathrm{A_{mr}}}{\mathrm{A_{sr}}} = \frac{\mathrm{r_m^2}\pi}{4\pi \mathrm{b}^2} \tag{2.5}$$

From that, the temperature change is

$$\Delta \mathrm{T} = \frac{\mathrm{P} * \eta * \mathrm{t}}{\mathrm{c} * \mathrm{m}} \tag{2.6}$$

with $\mathrm{c} = 600\,\frac{\mathrm{J}}{\mathrm{kgK}}$ being the specific heat capacity for glass, t the time and m the mass of the lid. No heat capacities for Macor are given and glass is the closest one.

The absorbed power of the lid is

$$\mathrm{P_{abs}} = \mathrm{P} * \eta \tag{2.7}$$

and

$$\mathrm{P_{ems}} = \mathrm{A_m} \sigma \mathrm{T_m^4} \epsilon \tag{2.8}$$

$\mathrm{A_m}$ is the surface of the lid, $\mathrm{T_m}$ the temperature and $\bar{\epsilon} = 0.9$ the average emissivity for Al_2O_3.

The oven will loose heat through the incoming wires, too. The calculation for the temperature loss follows as,

$$\Delta \mathrm{T} = \frac{\Delta \mathrm{W}}{\lambda \sigma} \mathrm{l} = \frac{\mathrm{I}^2 \rho_{\mathrm{cu}} \mathrm{l}^2 \Delta \mathrm{t}}{\lambda \sigma^2} \tag{2.9}$$

$\Delta \mathrm{W}$ describes the energy difference between the two points of interest, λ the heat conductance, σ the cross section for a wire with radius $\mathrm{r} = 0.25\,\mathrm{mm}$, $\mathrm{l} = 10\,\mathrm{mm}$ the distance between these points, I the current and ρ_{cu} the specific resistance of copper.

It would be also interesting to see how fast the wire would heat up at a specific current. For a wire with a diameter $d = 0.25\,\mathrm{mm}$ and a length of $l = 50\,\mathrm{cm}$, the resistance is

$$R = \frac{\rho l}{\sigma_a} = 0.04 \text{ Ohm}. \tag{2.10}$$

From this, the power of the wire for a current $I = 1\,\mathrm{A}$ is

$$P = I^2 R = 0.04\,\mathrm{Watt} \tag{2.11}$$

and an energy of

$$W = Pt = 0.04\,\mathrm{Joule} \tag{2.12}$$

With this value, the temperature change is

$$\Delta T = \frac{W}{c * m} = \frac{I^2 R \Delta t}{c * m} = 20 * \Delta t\,\mathrm{Kelvin} \tag{2.13}$$

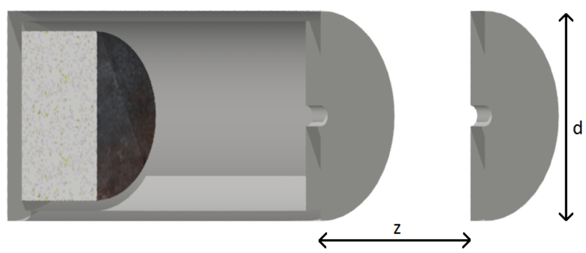

Figure 2.3: Half-section view of oven with aperture. The aperture is at a distance z from the oven nozzle. The material within the chamber corresponds to Ca granules. d denotes the diameter of the aperture.

Before the atomic beam enters the interaction region of the 2D-MOT, it must go through an aperture (see Figure 2.3).

$$\frac{d}{2} \leq r = z\frac{v_r}{v_z} \tag{2.14}$$

d describes the diameter of the aperture, r the radius of the atomic beam, z the distance between the oven output and the aperture, v_r the radial velocity and v_z the longitudinal velocity.

An integration over the radial dimension of the oven nozzle gives the number of atoms, which get through the aperture.

$$n_{total} = \int_{-r_{max}}^{r_{max}} \int_{0}^{v_{z,max}} dr dv_r np(v_z(v_r)) \tag{2.15}$$

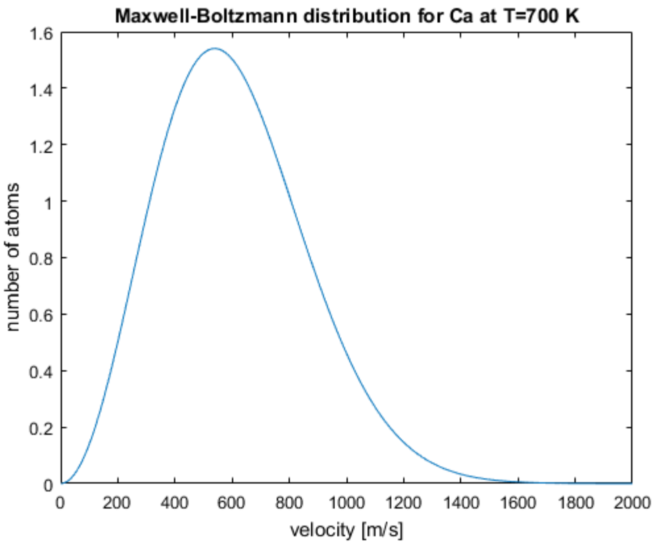

Figure 2.4: Maxwell-Boltzmann velocity distribution from the oven at a temperature of 800 K

$$p(v) = 4\pi \left(\frac{M}{2\pi k_B T}\right)^{3/2} v^2 \exp\left(-\frac{Mv^2}{2k_B T}\right) \tag{2.16}$$

$$v_z(v_r) = \frac{z}{r} v_r \tag{2.17}$$

n_{total} is the number of particles after the aperture, r_{max} the radius of the oven, $v_{z,max}$ the maximal longitudinal velocity, n the initial number density inside the oven and $p(v_z(v_r))$ the Maxwell-Boltzmann distribution.
When measuring the neutral fluorescence of the beam, coming out of the oven, it will be Doppler broadened. The increased full width at half maximum (FWHM) gives the mean temperature of the atoms [13],

$$T = \frac{m_0}{2\ln(2)k_B}\left(\frac{\Delta\omega c}{2\omega_0}\right), \tag{2.18}$$

with m_0 being the mass of ^{40}Ca, k_B the Boltzmann constant, $\Delta\omega$ the FWHM, c the speed of light and ω_0 the resonance frequency of Ca.
The maximum flux that can be extracted by a 2D-MOT is (see Ref. [28])

$$\Phi_c \approx \frac{1}{2}a_6\left(\frac{v_c}{\alpha}\right)n_s\bar{v}A\frac{\Omega_c}{4\pi}\,, \tag{2.19}$$

where a_6 denotes the natural abundance, v_c the capture velocity, $\bar{v}$ the mean velocity of the outcoming atomic beam, $\Omega_c = A_c/b$ the solid angle of capture with A_c as capture surface and b as distance between oven nozzle and interaction region of the MOT.

2.2 Experimental apparatus

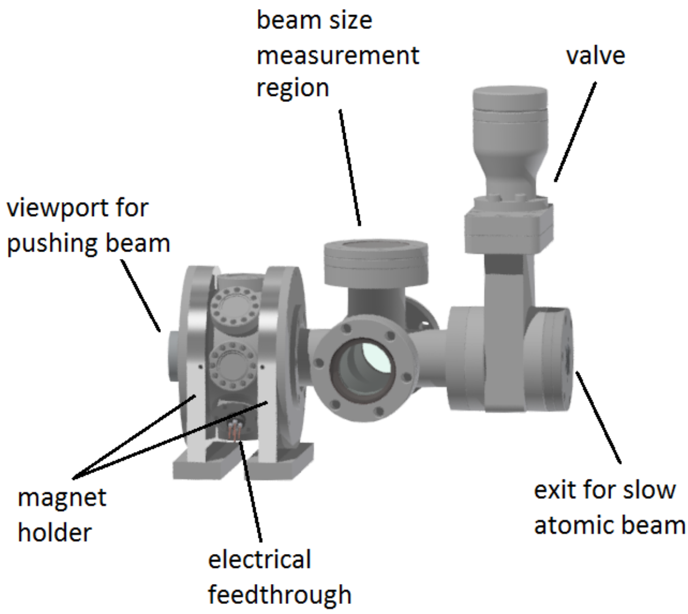

Figure 2.5: Assembly of the vacuum components. Permanent magnets inside the magnet holders produce a quadrupole-like field. The beam size measurement follows between the vacuum chamber and the valve. The valve allows the vacuum chamber to be attached to another chamber without venting. A power supply unit provides current for the heating wire through connection with the electrical feedthrough. A small viewport, on the side of the MOT-chamber, can be used for a pushing beam, if necessary.

The current limit of the electrical feedthrough is 5 A, as defined in the data sheet. The use of a consecutive turbo-molecular pump, between a rotary oil pump and the chamber achieves pressures of about 10^{-7} mBar.

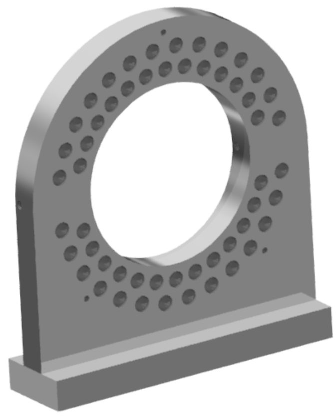

Figure 2.6: Layout of the magnet holder. The magnets and lid of the magnet holder are not shown in this figure. A total of 54 magnets fit inside this magnet holder. The gap between the upper and lower half of holes is due to two screws on the side of the magnet holder. The type of magnets used are called DE 610 with a remanence of $B_r \geq 1\,T$, a diameter of $d = 6\,mm$ and a length of $l = 10\,mm$.

The screws in Figure 2.6 serve the purpose of fixing the magnet rings at a certain distance from the center of the vacuum chamber.

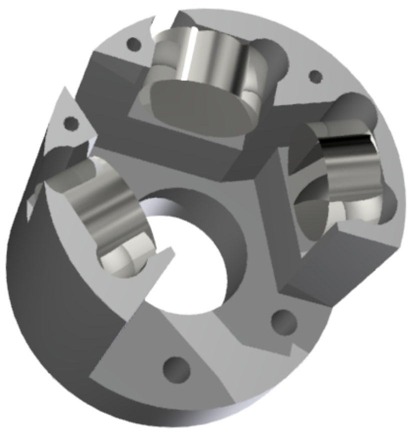

Figure 2.7: Layout of the mirror holder. The mirrors cause the beam to get retro-reflected on the right mirror. The overlapping beams at the center of the mirror holder are perpendicular to each other. The hole in the center of this mirror holder is due to imaging. If necessary, a pushing beam can be applied, too.

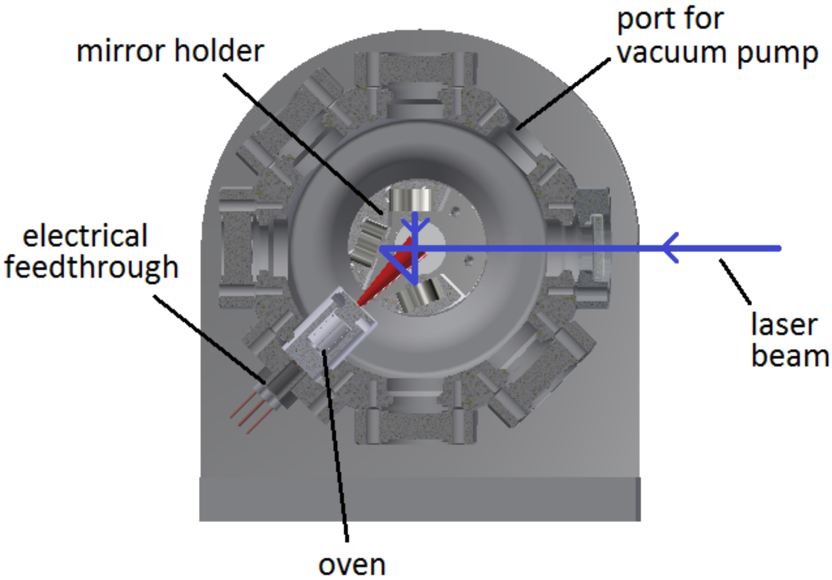

Figure 2.8: Half section view of the 2D-MOT chamber. The rings of permanent magnets (see Figure 2.5) have the same distance to the center of the chamber. On the top-right port of the chamber, a vacuum pump can be attached. The oven is unique and especially made to fulfill the needs of this project, like a long lifetime. The red cone describes the atoms coming out of the oven. The electrical feedthrough will be connected to a power supply for heating up the Constantan wire inside the oven.

2.3 The optical setup

In this section, I will explain the optical setup for the laser beams and how to lock the laser diode to a cavity.

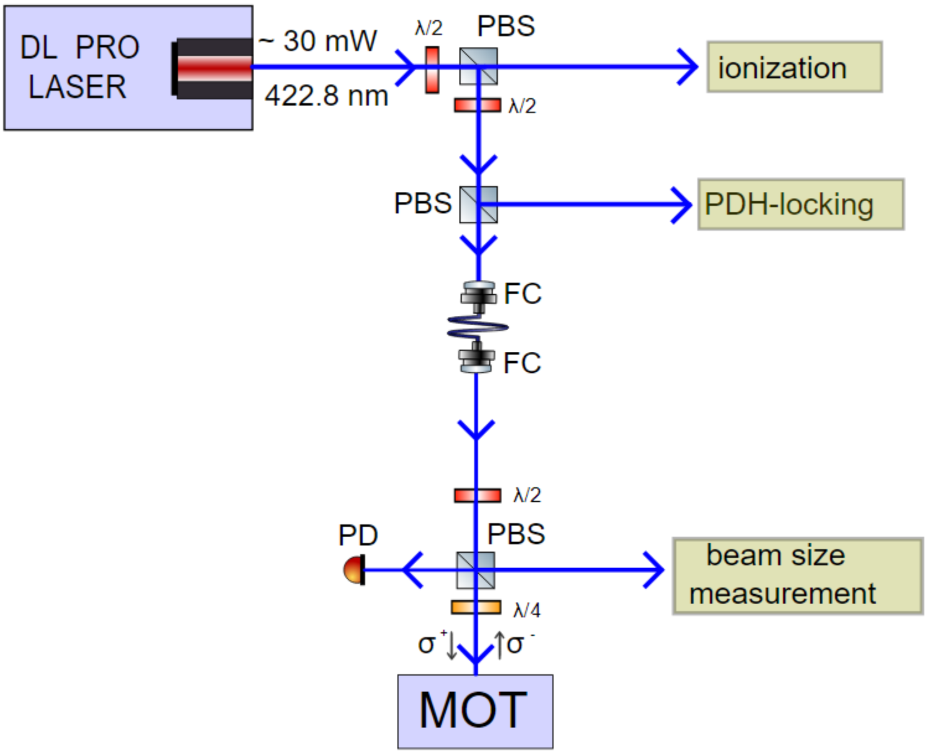

Figure 2.9: Schematics of the complete optical setup. PBS denotes the polarizing beam splitter, FC the fiber coupler and PD the photo diode. This figure consists of the pathway from the DL PRO laser source to the ionization, PDH-locking, beam size measurement and MOT- chamber. The $\frac{\lambda}{2}$ - wave plate rotates polarized light with respect to the incoming polarization of the beam. The $\frac{\lambda}{4}$ - wave plate circular polarizes incoming light, if the angle of the fast propagating axis is chosen to be 45° with respect to the incoming polarization of the beam.

2.3.1 PDH-Locking (Pound Drever Hall)

In this section, I will shortly explain how PDH-Locking works based on the work of E. D. Black [4].

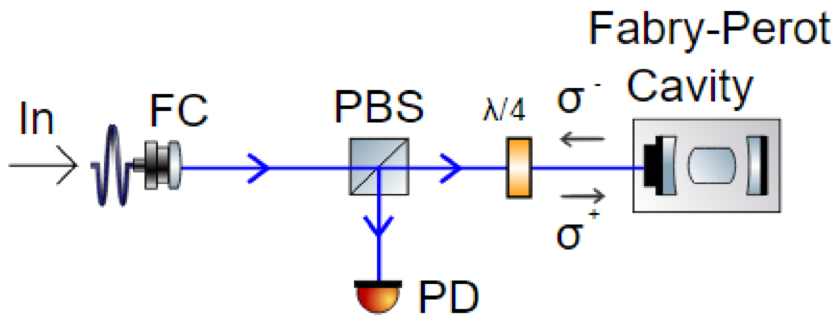

Figure 2.10: Schematics of PDH-Locking. The laser beam is circularly polarized within the Fabry-Perot-Cavity and therefore has another handedness after an odd number of reflections. The length of the cavity is adjusted in such a way that the desired wavelength fits inside. The PD is connected to a feedback loop, which regulates the laser current. A piezo changes the length of the cavity to tune the cavity frequency.

Normal frequency measurements are sensitive to intensity fluctuations. PDH - locking, on the other hand, is insensitive to laser intensity fluctuations. The reason for the use of PDH-Locking is that the laser frequency drifts over time due to temperature and current drifts. This is slow (h) due to a passive stability of the laser, because the current and temperature are set values. Those values can drift over time, tough. To avoid this, the laser must be locked to a reference cavity. To distinguish the direction of the drifting frequency, a so called error signal must be generated.

$$\epsilon = -\frac{4}{\pi}\sqrt{\mathrm{P_c P_s}}\frac{\delta\omega}{\delta\nu} \tag{2.20}$$

$\mathrm{P_c}$ denotes the power of the carrier frequency, $\mathrm{P_s}$ the power of the side bands, $\delta\omega$ the offset from resonance and $\delta\nu$ the cavity linewidth.

This error signal is antisymmetric around resonance with respect to the detuning between the cavity frequency and the laser frequency. To generate it, the incoming beam must be phase - modulated via an EOM (Electro

Optical Modulator). An electrical signal changes the refractive index of an EOM. This generates side modes to distinguish between the direction of the drifts. If the laser frequency changes, the intensity on the photo detector decreases, which in turn will regulate the laser frequency via a feedback loop. With this technique, an accuracy, compared to detuning stability of the laser beam, in the sub-Hz regime is achieved.

2.3.2 Scanning of laser frequency

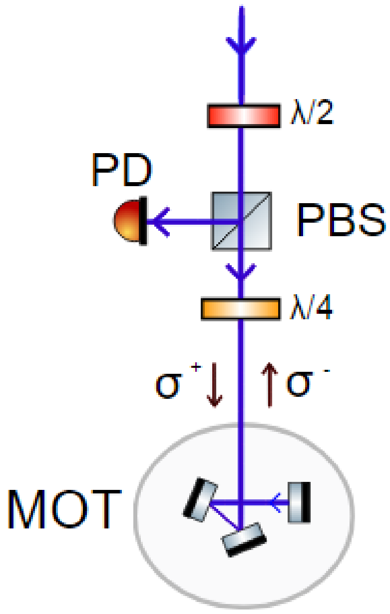

Figure 2.11: Schematics of optical setup in front of the vacuum chamber. It consists of a $\frac{\lambda}{2}$ - wave plate, $\frac{\lambda}{4}$ - wave plate, polarizing beam splitter and photo diode. The photo diode is used to detect the intensity of the laser beam, which comes out of the chamber.

The incoming light can either be right-handed or left- handed circular polarized. Within the MOT chamber, the light gets reflected five times, which will lead to an opposite circular polarization in contrast to the incoming beam.

This beam gets reflected at the PBS and therefore detected by the PD. This setup can be used to find the resonance of the cooling transition. As soon as the frequency of the laser beam is close to the resonance frequency of the Ca atoms, photon absorption occurs and a drop in intensity at the photo diode can be observed.
To get most knowledge about the system, the losses of the optical components must be included.
The laser power at the photo diode is

$$\mathrm{P_{out}} = \eta * \mathrm{P_{in}}, \tag{2.21}$$

with

$$\eta = |\mathrm{R_M}|^5 * |\mathrm{T_{WP}}|^2 * |\mathrm{T_{VP}}|^2 * |\mathrm{R_{PBS}}|$$

η denotes the efficiency of the optical setup after the beam splitter to the photo diode, R_M the reflection coefficient of the mirror $\mathrm{T_{WP}}$ the transmission coefficient of the wave plate, $\mathrm{T_{VP}}$ the transmission coefficient of the viewport, $\mathrm{R_{PBS}}$ the reflection coefficient of the polarizing beam splitter and $\mathrm{P_{in}}$ the power of the incoming laser beam.
This effect is hard to see at small laser currents ($\approx$ mA). Another possibility is to observe the fluorescence of atoms directly with a photo diode at the port for the pushing beam.
It is interesting to take a look at the size of the beam inside the mot, because the beam after the first reflection inside the chamber could cross the interaction region. This reduces the efficiency of the MOT.

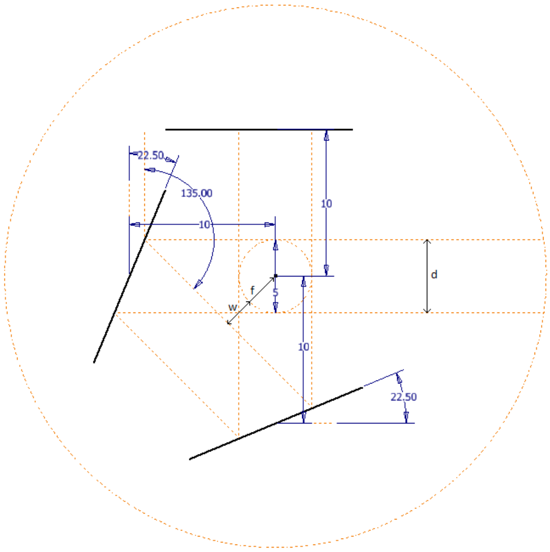

Figure 2.12: Beam path within the MOT. The black lines describes the position of the mirrors, the outer yellow-dotted circle the diameter of the mirror holder, the two yellow-dotted parallel lines the laser beam and the yellow-dotted inner circle the size of the interaction region of the incoming with the retro-reflected beam. The spacing between the interaction region and the reflected beam after the first reflection is denoted by w. d is the diameter of the beam. The distance between the center of the mirrors and the center of the interaction region a is 10 mm.

The geometrical calculation of the maximum allowed beam size gives

$$w = (f - r) - r = \frac{a}{\sqrt{2}} - 2r, \tag{2.22}$$

with a being the

Chapter 3

Simulation

In this section, I will go through the simulation and assumptions for it. Atom-atom and Photon-atom interactions describe the motion of atoms within the interaction region of a MOT. One way to calculate the atom-atom interaction is via diffusion. The problem that arises is that there is no steady-state temperature within a 2D-MOT and therefore no diffusion formula. Thus a Monte-Carlo simulation must be used for an atom-atom interaction. The simulated collision rate per second for an atom-atom interaction is in the order of 10^{-3}. Therefore, this kind of interaction has no big influence on the path of the atoms and is negliable. The simulation assumes no atom-atom interaction, but atoms interacting with light in a semi-classical model. The following additional assumptions are made:

- If the transition probability of a beam in x-direction, either + or -, is higher than the probability of a beam in y-direction, the probability for a transition, caused by a beam in y-direction, is set to zero and vice versa. The same applies to beams on the same axis. Otherwise, simultaneous excitation is possible.

- If a transition occurs, the spontaneous emission follows after 1 μs.
- After 10 ms, the simulation stops. The simulation will take several minutes, if this time is longer.
- the whole oven nozzle is a circle with diameter d = 1 mm.
- the beams are Gaussian.
- the incoming beam has a certain spread.
- the interaction region is spherical.
- for shorter calculation time, only 100 atoms are simulated.

The number of atoms that are entering the interaction region of the MOT (Eq. 2.19), for T = 923 K and m = 1 g is

$$\Phi_{\text{angle}} = 1.47 * 10^{11}\,\frac{1}{\text{s}}\,. \tag{3.1}$$

For these parameters the lifetime is around

$$\text{t}_{\text{oven}} = 10000\,\text{h}\,(\approx\; 416\,\text{days})\,. \tag{3.2}$$

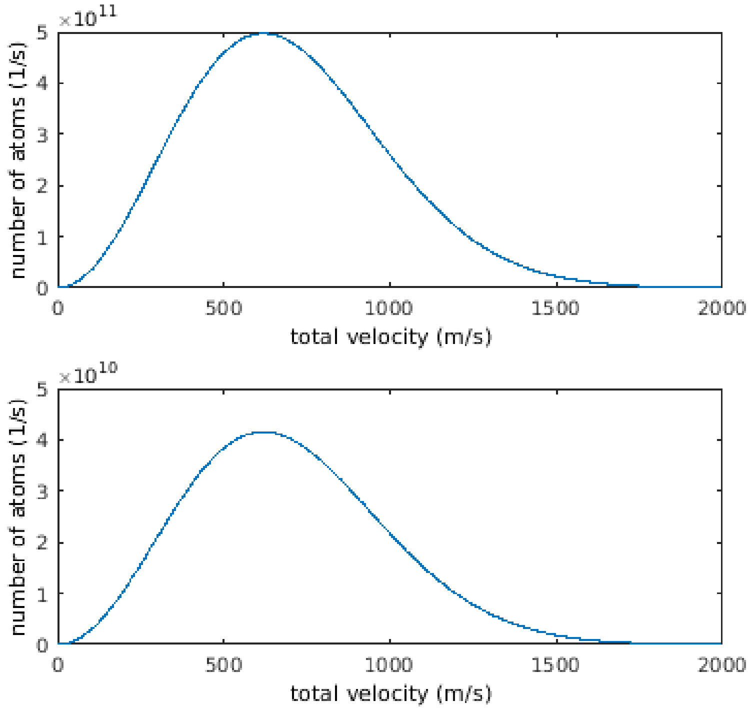

Figure 3.1: The upper figure displays the velocity distribution of atoms between the oven nozzle and the aperture nozzle. The second figure shows the velocity distribution of atoms after the aperture nozzle.

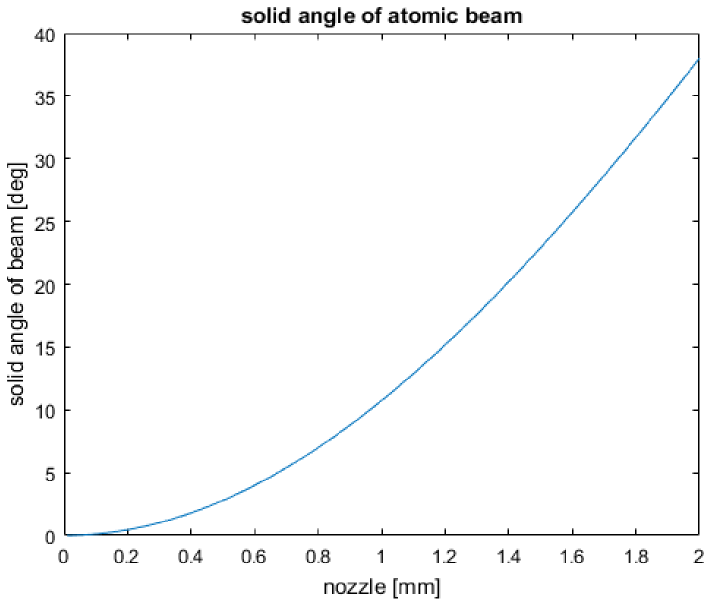

Figure 3.2: Solid angle of atomic beam coming out of the oven over aperture diameter.

The probability of an atom absorbing a photon is

$$\mathrm{P_{transition}} = \frac{\arctan(\frac{\mathrm{t}}{\gamma_{\mathrm{mod}}})}{\pi} + 0.5\,, \tag{3.3}$$

where t is the time between transitions and γ_{mod} the modified linewidth. It describes a cumulative Cauchy distribution [?].

The modified linewidth depends on the position and velocity of the particle and is given by

$$\gamma_{\mathrm{mod}} = \frac{\mathrm{s}\gamma}{2(1+\mathrm{s}+4\left(\frac{\delta_\pm}{\gamma}\right)^2)}\,, \tag{3.4}$$

where γ is the natural line width of ^{40}Ca, given by $\gamma = 34.5\,\mathrm{MHz}$, s the saturation parameter and δ the detuning.

The saturation intensity is $I_0 = 93.4\,\frac{\mathrm{mW}}{\mathrm{m^2}}$.

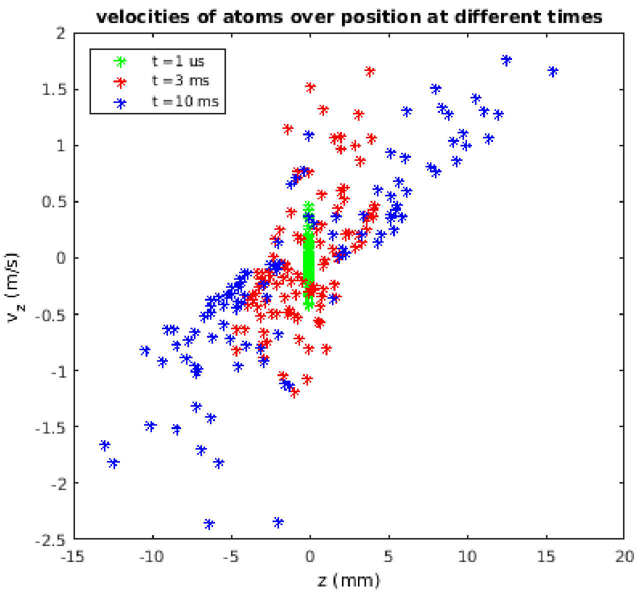

Figure 3.3: Monte-Carlo simulation of velocities of 100 atoms along the z-axis within the interaction region of MOT. After $1\,\mu s$, all atoms are confined at z ≈ 0 with a small velocity distribution in v_z going from ≈ -0.5 m/s to ≈ +0.5 m/s. After 3 ms the atoms are further distributed along the z-axis and also along v_z. At the end of the simulation the spacial and velocity distribution is the furthest, going from z ≈ -15 mm to z ≈ 15 mm and v_z from ≈ -2.5 m/s to +2 m/s.

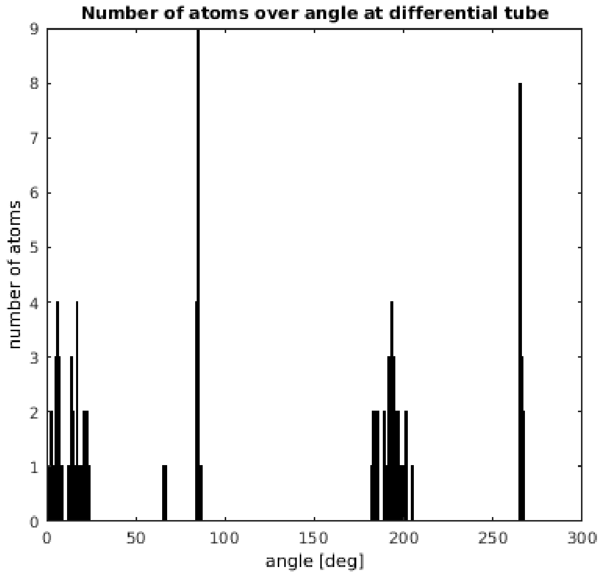

Figure 3.4: Number of atoms over angle in respect to direction from the oven nozzle to the center of the interaction region of the MOT with $\frac{\partial B}{\partial x} = 50\,\mathrm{Gs/cm}$. In the angles from 0 to $\approx 30\,°$, only atoms that were to fast and therefore left the interaction region on the other side of the incoming ones, are shown. At 90 and 270 ° , which are the $\pm$ z-directions, the atoms are very well collimated, which indicates that the simulation of the MOT works quite well. At 180 °, the atoms have not entered the interaction region, because those were to slow before the simulation stopped. The number of atoms going through the differential pumping tube in this simulation gives an efficiency of $\approx 3\,\%$.

The value for the temperature change is (see Eq. (2.6))

$$\Delta T \;=\; 0.8 * t\, Kelvin\,. \tag{3.5}$$

This means, if i do not take the emission of the lid into account, it would heat up to a temperature of 700 K in 10 minutes.

The resulting steady-state temperature is

$$T_m \;=\; 603\, Kelvin\,. \tag{3.6}$$

The calculation of the heat loss through the incoming wires (see Eq. (2.9)) gives

$$\Delta T \;=\; 4\, Kelvin\,. \tag{3.7}$$

For w = 0 and a = 10 mm the distance between the center of the interaction region and the mirror in Eq. (2.22), the beam diameter must be smaller than

$$d_{beam} \;=\; 7.1\, mm\,. \tag{3.8}$$

The magnetic field gradient simulation (see Ref. [3]) assumes two axially magnetized rings of permanent magnets and gives

$$\nabla \mathrm{B} \;=\; 85.4\,\mathrm{Gs/cm}\,. \tag{3.9}$$

Chapter 4

Measurement results

Table 4.1: Reflexion(R) and transmission(T) coefficients of optical components

Part	**Data sheet value**	**Experimental value**
PBS	$R_{PBS} > 0.99$	$R_{PBS} = 0.95$
Viewport	$T_{VP} \approx 0.92$	$T_{VP} = 0.92$
$\lambda/4$	$T_{WP} > 0.99$	$T_{WP} = 0.99$
Mirror (423 nm)	$R_M > 0.99$	$R_M = 0.98$

The results, for the efficiencies (see Eq. 2.3.2), are

$$\eta_{\text{theoretical}} > 0.79$$

and

$$\eta_{\text{experimental\_components}} = 0.73 \pm 0.02\,.$$

After setting up the optical setup, the measured efficiency gives

$$\eta_{\text{experimental}} = 0.79 \pm 0.02\,.$$

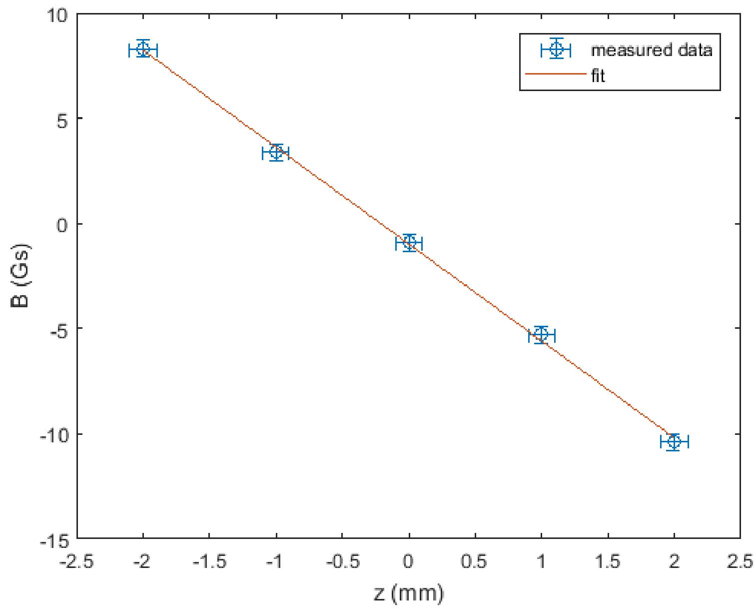

Figure 4.1: Measurement of magnetic field within vacuum chamber. The spacing between the measurement points is 1 mm.

The measurement of the magnetic field gradient gives

$$\nabla \mathrm{B} = (36.8 \pm 0.4)\,\mathrm{Gs/cm}\,.$$

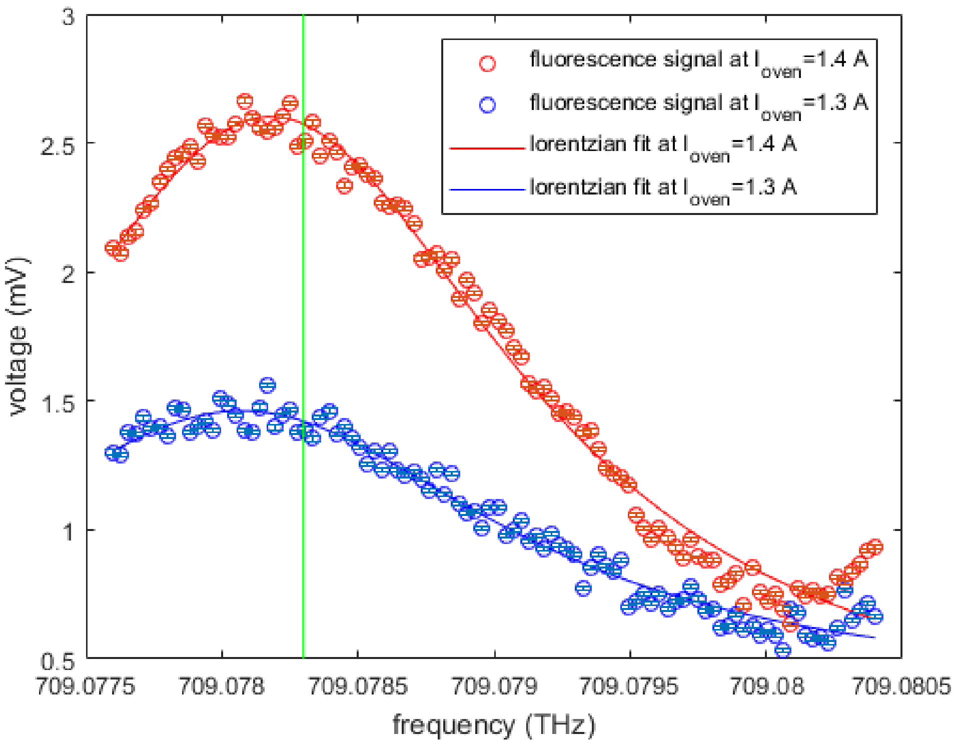

Figure 4.2: Plot of measurement signals and Lorentzian fits of neutral fluorescence at oven currents of 1.3 A (blue) and 1.4 A (red). The green line symbolizes the reference frequency at 709.0783 THz. The laser power inside the MOT is (3.79 ± 0.02) mW. The linewidth at FWHM gives $\Delta\lambda$=2.4749 GHz, which corresponds to a temperature of T = 951.7782 K.

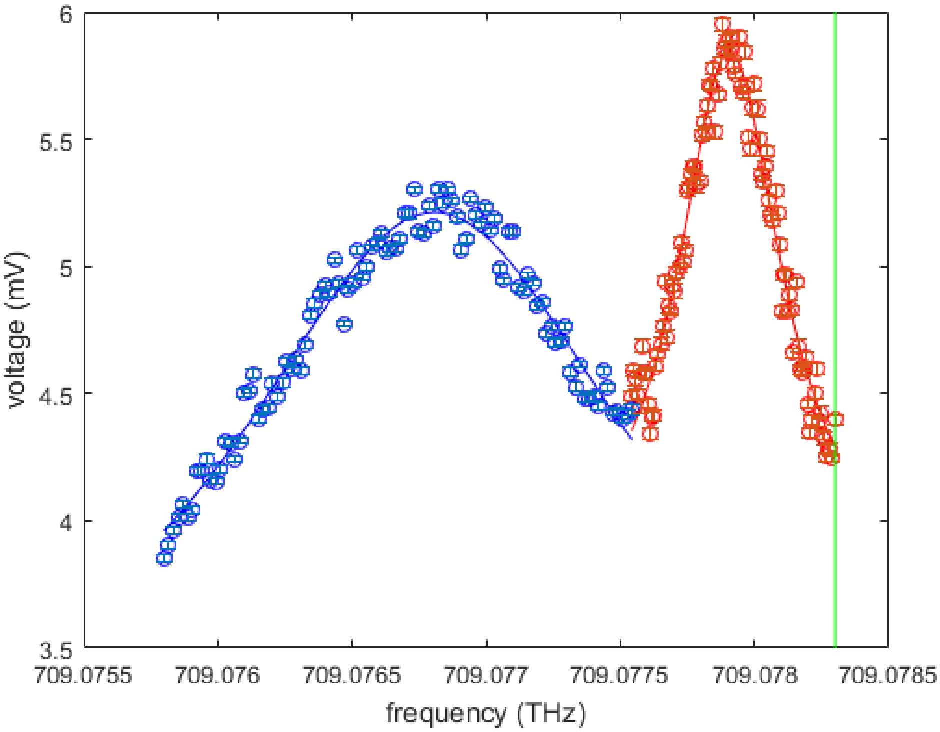

Figure 4.3: Plot of measurement signals and Lorentzian fits of neutral fluorescence. The laser power inside the MOT is (8.98 ± 0.02) mW. The green line symbolizes the reference frequency at 709.0783 THz. The center of the Doppler broadened signal (blue) is at 709.0768 THz. The center of the signal of cooled atoms (red) is at 709.0779 THz. This corresponds to a maximal signal at a detuning of 400 MHz. The oven current is 1.3 A. The linewidth for the cooled atoms at FWHM gives $\Delta\lambda \approx 1$ GHz, which corresponds to a temperature of $T \approx 155$ K.

Figure 4.4: Observed fluorescence of 2D-MOT. The bright spot in the middle of the crossing beams comes from either over saturation of the camera or confined atoms within the interaction region.

Summary and outlook

I presented a pure 2D-MOT as suitable candidate for loading ion traps. The use of permanent magnet rings with a resulting gradient of $\nabla B = (36.8 \pm 0.4)\,\mathrm{Gs/cm}$ is enough to observe fluoresence (see Figure 4.4). The difference to the simulation $\nabla \mathrm{B} = 85.4\,\mathrm{Gs/cm}$ could be due to the magnet holder material (Aluminium). This needs further investigation. The design of a novel oven design gives satisfying results at currents above $\approx 1\,\mathrm{A}$. One should be careful about not using currents above 1.5 A, due to breaking the wire. The temperature calculated from Figure 4.2 via Eq. (2.18) is at the estimated value of 600 °C. To decrease the error, a higher laser intensity, or better detection e.g. via photo multiplier tube, is required. The temperature of the cold atoms within the MOT (see Figure 4.3) is $\mathrm{T} \approx 155\,\mathrm{K}$.

The estimated value for the oven lifetime $\mathrm{t} = 10000\,\mathrm{h}$ assumes atoms directly leaving the oven. Therefore, this value is rather a lower limit than the estimated value.

The difference between the two experimental efficiencies $\eta_{\mathrm{experimental\_components}} = 0.73 \pm 0.02$ and $\eta_{\mathrm{experimental}} = 0.79 \pm 0.02$ could be explained by the usage of different components for both measurements.

Acknowledgment

Appendices

Appendix A

Piezo driver

Most of the circuit has been copied from Frieder Lindenfelser's master thesis. Linear power supplies give a DC output of 200 V. They give a physical separation between the circuit and the power net. This allows to omit the parts for rectifying the input signal. Another change made is the use of a switch at the input of the operational amplifier. The linear power supply is able to drive three piezos at its maximum, because one operational amplifier needs less than 200 mA and the power supply gives 600 mA. Four piezos are used for the eQual project.

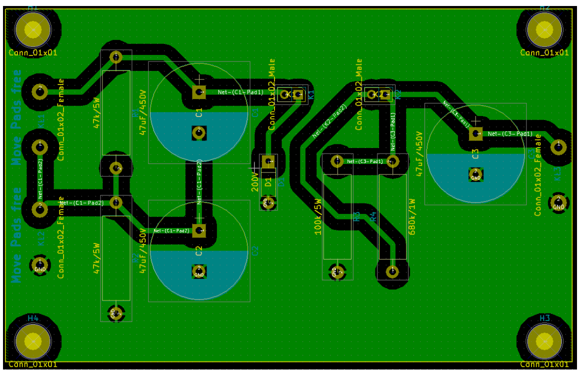

Figure A.1: PCB-design of power supply circuitr

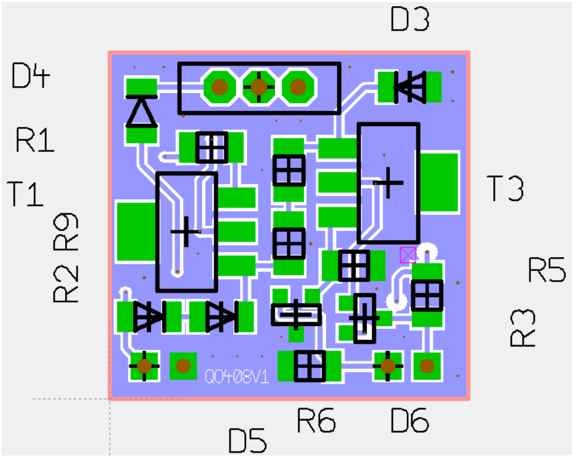

Figure A.2: PCB-design of voltage increasing circuit

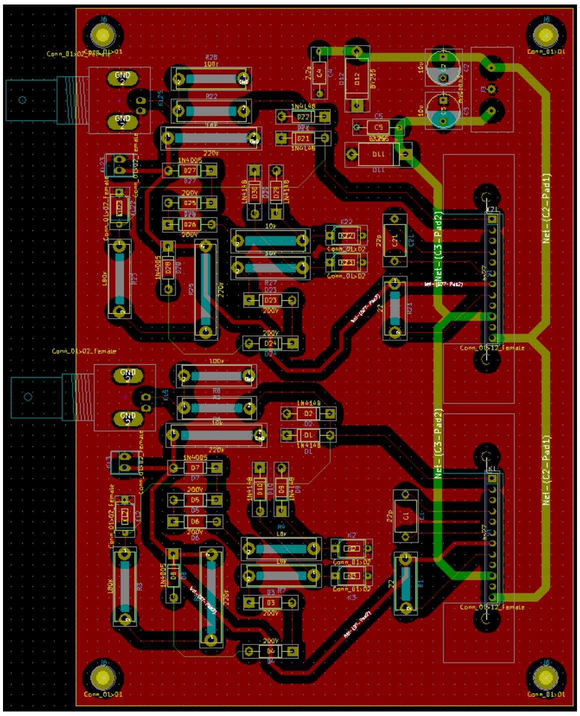

Figure A.3: PCB-design of opamp circuit

To be able to drive a piezo, one needs three circuits. The first one (see Figure A.1) is for rectifying the input voltage and setting the output voltage. The rectification is obsolete, because a linear power supply is used and therefore

R1, R2, C1 and C2 can be omitted. The second PCB (see Figure A.2) increases the input voltage to the desired value of approximately 400 V. The third one (see Figure A.3) is the operational amplifier circuit.

Bibliography

[1] C.B. Alcock. Vapor pressure of the metallic elements, 2000.

[2] Muhammad Anwar, Daniel V Magalhães, Stella T Müller, Muhammad Faisal, Muhammad Nawaz, and Mushtaq Ahmed. Revisiting the capture velocity of a cesium magneto-optical trap: model, simulation and experiment. *Laser Physics*, 24(12):125502, 2014.

[3] S.I. Babic and C. Akyel. Improvement in the analytical calculation of the magnetic field produced by permanent magnets. 2008.

[4] Eric D. Black. An introduction to pound–drever–hall laser frequency stabilization. *American Journal of Physics*, 69(1):79–87, jan 2001.

[5] R. Blatt, W. Ertmer, P. Zoller, and J. L. Hall. Atomic-beam cooling: A simulation approach. *Physical Review A*, 34(4):3022–3033, oct 1986.

[6] P. M. Bota, D. Dorobantu, I. Boerasu, D. Bojin, and M. Enachescu. New laser ablation chamber for producing carbon nanomaterials using excimer laser. *Materials Research Innovations*, 19(1):33–39, may 2014.

[7] Colin D. Bruzewicz, Robert McConnell, John Chiaverini, and Jeremy M. Sage. Scalable loading of a two-dimensional trapped-ion array. *Nature Communications*, 7:13005, sep 2016.

[8] P. Cheiney, O. Carraz, D. Bartoszek-Bober, S. Faure, F. Vermersch, C. M. Fabre, G. L. Gattobigio, T. Lahaye, D. Guéry-Odelin, and R. Mathevet. A zeeman slower design with permanent magnets in a halbach configuration. *Review of Scientific Instruments*, 82(6):063115, jun 2011.

[9] U Dammalapati, I Norris, L Maguire, M Borkowski, and E Riis. A compact magneto-optical trap apparatus for calcium. *Measurement Science and Technology*, 20(9):095303, jul 2009.

[10] C. J. Dedman, J. Nes, T. M. Hanna, R. G. Dall, K. G. H. Baldwin, and A. G. Truscott. Optimum design and construction of a zeeman slower for use with a magneto-optic trap. *Review of Scientific Instruments*, 75(12):5136–5142, dec 2004.

[11] K. Dieckmann, R. J. C. Spreeuw, M. Weidemüller, and J. T. M. Walraven. Two-dimensional magneto-optical trap as a source of slow atoms. *Physical Review A*, 58(5):3891–3895, nov 1998.

[12] Pradip K. Ghosh. *Ion Traps (International Series of Monographs on Physics)*. Clarendon Press, 1996.

[13] Hermann Haken and Hans Christoph Wolf. *The Physics of Atoms and Quanta*. Springer Berlin Heidelberg, 1996.

[14] Michael A. Joffe, Wolfgang Ketterle, Alex Martin, and David E. Pritchard. Transverse cooling and deflection of an atomic beam inside a zeeman slower. *Journal of the Optical Society of America B*, 10(12):2257, dec 1993.

[15] Prem Kumar, G. Mauro D'Ariano, Osamu Hirota, Jeffrey H. Shapiro, and Horace P. Yuen. *Quantum Communication, Computing, and Measurement 2 (v. 2)*. Springer, 2000.

[16] P. D. Lett, W. D. Phillips, S. L. Rolston, C. E. Tanner, R. N. Watts, and C. I. Westbrook. Optical molasses. *Journal of the Optical Society of America B*, 6(11):2084, nov 1989.

[17] Harold J. Metcalf, Peter van der Straten, and Peter van der Straten. *Laser Cooling and Trapping (Graduate Texts in Contemporary Physics)*. Springer, 2001.

[18] Peter W. Milonni and Joseph H. Eberly. *Lasers (Wiley Series in Pure and Applied Optics)*. Wiley-Interscience, 1988.

[19] J Mitroy. Energy levels and oscillator strengths for neutral calcium. *Journal of Physics B: Atomic, Molecular and Optical Physics*, 26(21):3703, 1993.

[20] Ian Norris. Laser cooling and trapping of neutral calcium atoms, 2009.

[21] Ingo Nosske, Luc Couturier, Fachao Hu, Canzhu Tan, Chang Qiao, Jan Blume, Y. H. Jiang, Peng Chen, and Matthias Weidemüller. Two-dimensional magneto-optical trap as a source for cold strontium atoms. *Physical Review A*, 96(5), nov 2017.

[22] William D. Phillips and Harold Metcalf. Laser deceleration of an atomic beam. *Physical Review Letters*, 48(9):596–599, mar 1982.

[23] E. J. Salumbides, V. Maslinskas, I. M. Dildar, A. L. Wolf, E.-J. van Duijn, K. S. E. Eikema, and W. Ubachs. High-precision frequency measurement of the 423-nm ca i line. *Physical Review A*, 83(1), jan 2011.

[24] J. Schoser, A. Batär, R. Löw, V. Schweikhard, A. Grabowski, Yu. B. Ovchinnikov, and T. Pfau. Intense source of cold rb atoms from a pure two-dimensional magneto-optical trap. *Physical Review A*, 66(2), aug 2002.

[25] C.A. Schrama, E. Peik, W.W. Smith, and H. Walther. Novel miniature ion traps. *Optics Communications*, 101(1-2):32–36, aug 1993.

[26] Stig Stenholm. The semiclassical theory of laser cooling. *Reviews of Modern Physics*, 58(3):699–739, jul 1986.

[27] Utako Tanaka, Kensuke Suzuki, Yuki Ibaraki, and Shinji Urabe. Design of a surface electrode trap for parallel ion strings. *Journal of Physics B: Atomic, Molecular and Optical Physics*, 47(3):035301, 2014.

[28] T. G. Tiecke, S. D. Gensemer, A. Ludewig, and J. T. M. Walraven. High-flux two-dimensional magneto-optical-trap source for cold lithium atoms. *Physical Review A*, 80(1), jul 2009.

[29] John W. Ward and Malcolm V. Fraser. Some of the parameters affecting knudsen effusion. IV. monte carlo calculations of effusion probabilities and flux gradients for knudsen cells. *The Journal of Chemical Physics*, 49(9):3743–3750, nov 1968.

[30] W. L. Winterbottom. Vapor—solid interactions and the effusion oven. i. the total effusion current through a cylindrical orifice. *The Journal of Chemical Physics*, 47(9):3546–3556, nov 1967.